$K^*(892)^0$ and $\bar{K}^*(892)^0$ production in central Pb + Pb, Si + Si, C + C, and inelastic $p + p$ collisions at 158A GeV

T. Anticic,[22] B. Baatar,[8] D. Barna,[4] J. Bartke,[6] H. Beck,[9] L. Betev,[10] H. Białkowska,[19] C. Blume,[9] M. Bogusz,[21] B. Boimska,[19] J. Book,[9] M. Botje,[1] P. Bunčić,[10] T. Cetner,[21] P. Christakoglou,[1] P. Chung,[18] O. Chvala,[14] J. G. Cramer,[15] V. Eckardt,[13] Z. Fodor,[4] P. Foka,[7] V. Friese,[7] M. Gaździcki,[9,11] K. Grebieszkow,[21] C. Höhne,[7] K. Kadija,[22] A. Karev,[10] V. I. Kolesnikov,[8] M. Kowalski,[6] D. Kresan,[7] A. Laszlo,[4] R. Lacey,[18] M. van Leeuwen,[1] M. Mackowiak,[21] M. Makariev,[17] A. I. Malakhov,[8] M. Mateev,[16] G. L. Melkumov,[8] M. Mitrovski,[9] S. Mrówczyński,[11] V. Nicolic,[22] G. Pálla,[4] A. D. Panagiotou,[2] W. Peryt,[21] J. Pluta,[21] D. Prindle,[15] F. Pühlhofer,[12] R. Renfordt,[9] C. Roland,[5] G. Roland,[5] M. Rybczyński,[11] A. Rybicki,[6] A. Sandoval,[7] N. Schmitz,[13] T. Schuster,[9] P. Seyboth,[13] F. Siklér,[4] E. Skrzypczak,[20] M. Słodkowski,[21] G. Stefanek,[11] R. Stock,[9] H. Ströbele,[9] T. Susa,[22] M. Szuba,[21] M. Utvić,[9] D. Varga,[3,4] M. Vassiliou,[2] G. I. Veres,[4,5] G. Vesztergombi,[4] D. Vranić,[7] Z. Włodarczyk,[11] and A. Wojtaszek-Szwarc[11]

(The NA49 collaboration)

[1]*NIKHEF, Amsterdam, Netherlands*
[2]*Department of Physics, University of Athens, Athens, Greece*
[3]*Eötvös Loránt University, Budapest, Hungary*
[4]*KFKI Research Institute for Particle and Nuclear Physics, Budapest, Hungary*
[5]*MIT, Cambridge, Massachusetts, USA*
[6]*Henryk Niewodniczanski Institute of Nuclear Physics, Polish Academy of Sciences, Cracow, Poland*
[7]*GSI Helmholtzzentrum für Schwerionenforschung, Darmstadt, Germany*
[8]*Joint Institute for Nuclear Research, Dubna, Russia*
[9]*Fachbereich Physik der Universität, Frankfurt, Germany*
[10]*CERN, Geneva, Switzerland*
[11]*Institute of Physics, Jan Kochanowski University, Kielce, Poland*
[12]*Fachbereich Physik der Universität, Marburg, Germany*
[13]*Max-Planck-Institut für Physik, Munich, Germany*
[14]*Charles University, Faculty of Mathematics and Physics, Institute of Particle and Nuclear Physics, Prague, Czech Republic*
[15]*Nuclear Physics Laboratory, University of Washington, Seattle, Washington, USA*
[16]*Atomic Physics Department, Sofia University Saint Kliment Ohridski, Sofia, Bulgaria*
[17]*Institute for Nuclear Research and Nuclear Energy, Sofia, Bulgaria*
[18]*Department of Chemistry, Stony Brook Univ. (SUNYSB), Stony Brook, New York, USA*
[19]*Institute for Nuclear Studies, Warsaw, Poland*
[20]*Institute for Experimental Physics, University of Warsaw, Warsaw, Poland*
[21]*Faculty of Physics, Warsaw University of Technology, Warsaw, Poland*
[22]*Rudjer Boskovic Institute, Zagreb, Croatia*

(Received 31 May 2011; revised manuscript received 30 September 2011; published 13 December 2011)

Production of the $K^*(892)^0$ and $\overline{K}^*(892)^0$ resonances was studied via their $K^+\pi^-$ and $K^-\pi^+$ decay modes in central Pb + Pb, Si + Si, C + C, and inelastic $p + p$ collisions at 158A GeV($\sqrt{s_{NN}} = 17.3$ GeV) with the NA49 detector at the CERN SPS. Transverse momentum and rapidity distributions were measured and total yields were estimated. The yield of K^* exceeds that of $\overline{K}^*$ by about a factor of two in nucleus-nucleus reactions. The total yield ratios $\langle K^*\rangle/\langle K^+\rangle$ and $\langle \overline{K}^*\rangle/\langle K^-\rangle$ are strongly suppressed in central Pb + Pb compared to $p + p$, C + C, and Si + Si collisions, in agreement with the expected attenuation of these short-lived resonance states in the hadronic phase of the expanding fireball. The UrQMD model, although incorporating such a scenario, does not provide a quantitative description of the experimental results. The statistical hadron gas model assuming the same freeze-out parameters for stable hadrons and resonances overestimates the $\langle K^*\rangle/\langle K\rangle$ ratios in central Pb + Pb collisions by about a factor of 2.5.

DOI: 10.1103/PhysRevC.84.064909 PACS number(s): 13.85.Ni, 25.75.Dw

I. INTRODUCTION

High-energy collisions of heavy nuclei produce a transient state of extreme energy and matter density in which quarks and gluons are probably briefly deconfined [1–3]. Production of entropy and of s, $\bar{s}$ quarks is believed to occur at the early stage of the collision and this process is expected to be sensitive to the phase of the created matter [4,5]. The high-density state evolves into a hadron-resonance gas which finally decouples into the observed hadrons. The $K^*(892)$ and $\overline{K}^*(892)$ resonance states contain a $\bar{s}$ and a s valence quark, respectively, and are therefore sensitive to the level of strangeness production. However, resonance states have lifetimes similar to that of the fireball and may interact in the dense medium in which they are produced. Their mass and width could be affected [6] and scattering processes might destroy or regenerate them. Furthermore, daughters of those

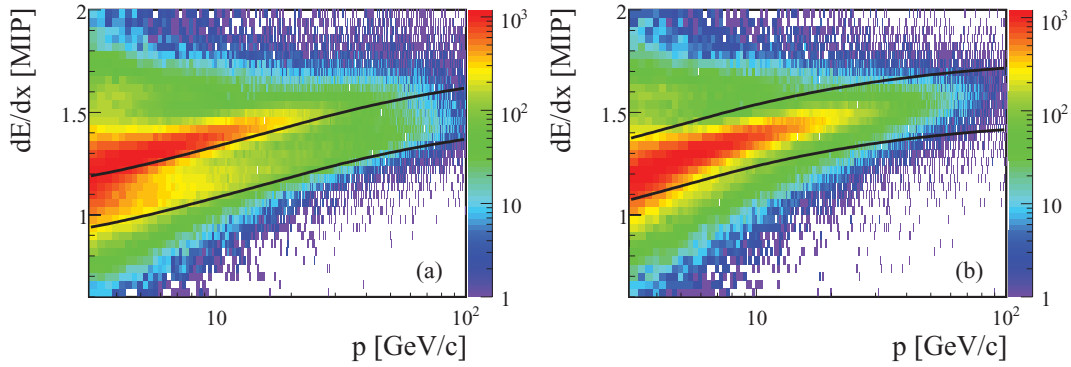

FIG. 1. (Color online) Specific energy loss dE/dx in units of minimum ionizing particles (MIP) measured in the NA49 TPCs versus momentum p for positively (a) and negatively (b) charged particles in central Pb + Pb collisions. Curves in (a) and (b) show the acceptance limits for K^+ and π^-, respectively.

K^* that decay inside the fireball may rescatter, resulting in a changed invariant-mass spectrum. Thus, the yields contained in the K^* mass peak were conjectured to be sensitive to the duration and properties of the hadronic fireball stage [7].

Studies of $K^*(892)$ production at midrapidity in Au + Au, Cu + Cu, and $p + p$ collisions at RHIC energies were performed by the STAR collaboration [8,9]. This paper reports measurements of $K^*(892)^0$ and $\overline{K}^*(892)^0$ resonance production via their $K^+\pi^-$ and $K^-\pi^+$ decay modes at the CERN SPS in central Pb + Pb, Si + Si, C + C, and inelastic $p + p$ collisions at 158A GeV($\sqrt{s_{NN}} = 17.3$ GeV). Preliminary results were presented in Ref. [10]. Section II briefly describes the NA49 detector. Section III discusses the analysis procedure. Distributions of transverse momentum p_T and center-of-mass rapidity y, as well as total yields, are presented in Sec. IV. These results are compared to predictions of the ultrarelativistic quantum molecular dynamics (UrQMD) model [11] and a statistical hadron gas model (HGM) [12] in Sec. V. The paper ends with the summary Sec. VI.

II. DETECTOR

The NA49 experimental apparatus [13] consists of four large-volume time projection chambers (TPCs). Two of these (VTPC) are placed in the fields of two superconducting dipole magnets. The other two (MTPC) are positioned downstream of the magnets and are optimized for high-precision measurements of the ionization energy loss dE/dx with a resolution of about 4%. The particle identification provided by the dE/dx measurement is complemented in the midrapidity domain by a measurement of the time of flight (TOF) with a resolution of about 60 ps in two TOF detector arrays positioned downstream of the MTPCs. The magnetic fields were set to about 1.5 T (upstream magnet) and 1.1 T (downstream magnet). With the lower momentum cut employed for dE/dx identification the detector acceptance covers the forward rapidity region for $K^*(892)$.

The precise transverse position of each beam particle at the target was measured by three pairs of small proportional wire chambers (BPD) upstream of the target with a precision of better than 200 μm. Lead ions of 158A GeV impinged on a thin Pb-foil target of 337 mg/cm^2 (approximately 1.5% interaction probability for Pb ions) which was positioned 80 cm upstream from the first VTPC. For the study of C + C and Si + Si collisions a 3-mm-thick C (2.4% interaction length) and 5-mm-thick Si target (4.4%) were used, respectively. The incident C and Si nuclei were produced by fragmentation of a Pb beam of 158A GeV beam energy [13] and were selected

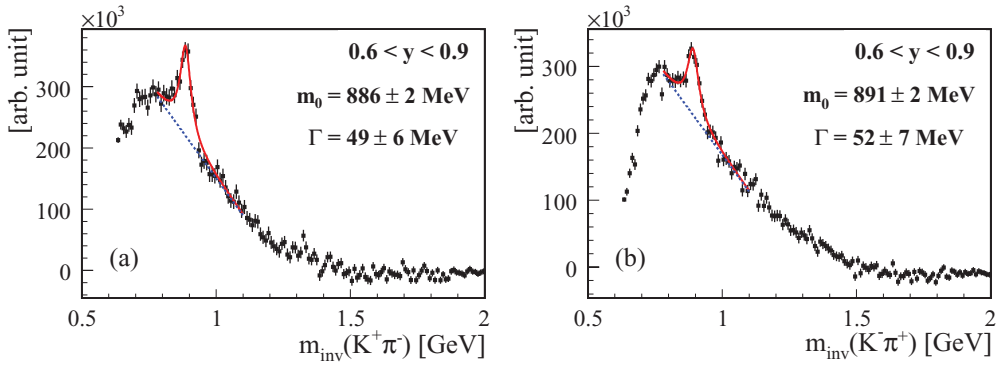

FIG. 2. (Color online) Invariant-mass distribution of $K^+\pi^-$ (a) and $K^-\pi^+$ (b) for $p_T < 2.0$ GeV/c in the rapidity region $0.6 < y < 0.9$ after subtraction of mixed-pair background in central Pb + Pb collisions. The fitted polynomial background is shown by the dashed curves; the sum of fitted polynomial background and signal Breit-Wigner function is shown by the solid curves.

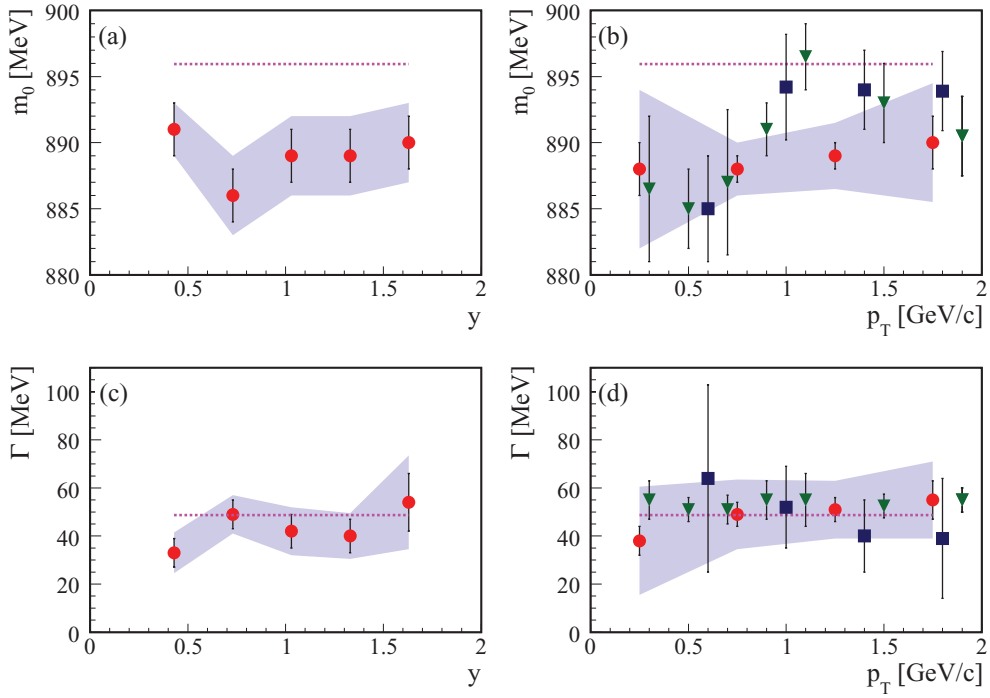

FIG. 3. (Color online) Fitted mass values m_0 (a),(b) and width Γ (c),(d) of the $K^*(892)^0$ peak in the $K^+\pi^-$ mass distribution versus rapidity y (a),(c) and transverse momentum p_T (b),(d) in central Pb + Pb collisions. Dots show the fitted values with statistical error bars, and bands indicate the systematic uncertainties. The dotted horizontal lines indicate the world average values for m_0 and Γ [19]. For comparison results are shown from the STAR collaboration at RHIC [9] for Au + Au collisions at $\sqrt{s_{NN}} = 62$ GeV (triangles) and $\sqrt{s_{NN}} = 200$ GeV (squares).

by magnetic rigidity ($Z/A = 0.5$) and by specific energy loss in the BPDs. The "C beam" as defined by the online trigger and offline selection was a mixture of ions with $Z = 6$ and 7 (intensity ratio 69:31); the "Si-Beam" was a mixture of ions with $Z = 13$, 14, and 15 (intensity ratio 35:41:24). The trigger selected the centrality of the collisions based on a measurement of the energy deposited by projectile spectator nucleons in a downstream calorimeter.

For the study of $p + p$ collisions the beam line was set to select secondary protons of 158 GeV/c momentum which were produced in a Be target by the 400 GeV/c SPS proton beam. The secondary protons were identified by Cherenkov counters in the H2 beamline, resulting in a contamination by pions and kaons of less then 10^{-3}. Liquid hydrogen targets of 14 cm (year 1996) and 20 cm (later years, 2.8% interaction length) and 3 cm diameter were used. A scintillation counter S4 of 2 cm diameter was positioned about 5 m downstream on the deflected beam line between the two VTPCs. It was used in anticoincidence with the beam to select $p + p$ interactions. For a detailed description of detector aspects for $p + p$ collisions, see Ref. [14].

III. DATA ANALYSIS

The analysis of Pb + Pb reactions is based on a high-statistics data run which recorded about 3×10^6 collisions. The trigger selected the 23.5% most central Pb + Pb collisions. The corresponding mean number of wounded nucleons N_w [15]

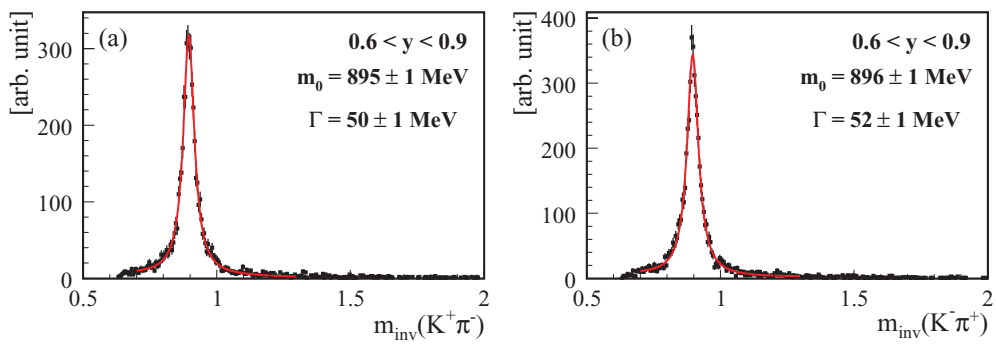

FIG. 4. (Color online) Invariant-mass spectra of simulated and embedded $K^*(892)^0$ (a) and $\overline{K}^*(892)^0$ (b) calculated from reconstructed matched tracks.

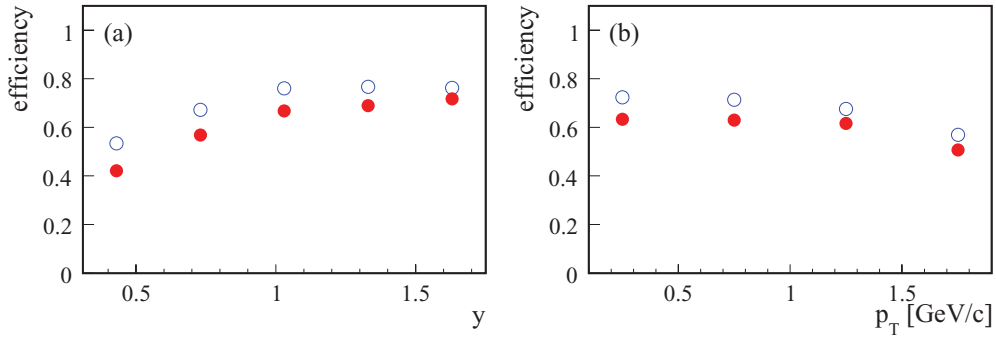

FIG. 5. (Color online) Combined reconstruction efficiency and acceptance of $K^*(892)^0 \to K^+\pi^-$ as a function of rapidity (transverse momentum range $0 < p_T < 2.0$ GeV/c) (a) and transverse momentum (rapidity range $0.43 < y < 1.78$) (b) in central Pb + Pb collisions. Solid and open symbols show results with and without embedding into real events (see text). The decay branching ratio is not included in the plotted efficiencies.

was calculated using the VENUS simulation code [16] following the Glauber model approach and found to be $\langle N_w \rangle = 262$ with a systematic uncertainty of ± 5. More details on the procedure can be found in Ref. [17].

The C + C and Si + Si collision data are more limited in statistics. For both systems about 45×10^3 events were recorded for the $(15.3 \pm 2.4)\%$ and $(12.2 \pm 1.8)\%$ most central C + C and Si + Si collisions, respectively. The corresponding mean numbers of wounded nucleons obtained from VENUS simulations are 14 ± 2 and 37 ± 3 [18].

Results on $p + p$ reactions are based on 1.125×10^6 (4.18×10^5) events collected with a 20 (14)-cm-long liquid hydrogen target. The trigger cross section was 28.3 ± 0.1 mb which represents about 86% of the inelastic cross section and excludes most of the elastic collisions (about 1 mb remaining contamination) [14].

Charged-particle tracks were reconstructed from the charge deposited along the particle trajectories in the TPCs using a global tracking scheme which combines track segments that belong to the same physical particle but were detected in different TPCs. A vertex fit was then performed using the reconstructed tracks. Particle identification is based on measurements of the 50% truncated mean of the specific energy loss dE/dx in the TPCs which provide up to 234 charge samples on a track. The uncertainty of the dE/dx measurement for a specific track depends on its visible length and the number of associated charge clusters. The average value of dE/dx is a universal function of the velocity of a charged particle (Bethe-Bloch curve) and thus depends on its mass for a given momentum.

A. Pb + Pb collisions

For Pb + Pb collisions the event vertex was determined using the tracks reconstructed in the TPCs. The resulting vertex distribution had widths $\sigma(x) = 0.21$ cm and $\sigma(y) = 0.15$ cm in the coordinates transverse to the beam, and $\sigma(z) = 1.3$ cm in the longitudinal direction. Events were accepted, if the vertex z coordinate was within 1 cm of the nominal target position. With this requirement the background from nontarget interactions was negligible. Further cuts were applied at the track level. The distance of the backextrapolated track from the fitted vertex position had to be below 5 cm in the (horizontal) bending plane and below 3 cm in the vertical direction. Moreover, the number of measured points on the track had to exceed 25 and constitute more than 50% of the geometrically possible maximum to eliminate split tracks. Finally, the track momentum fit was repeated including the vertex position resulting in a typical momentum resolution

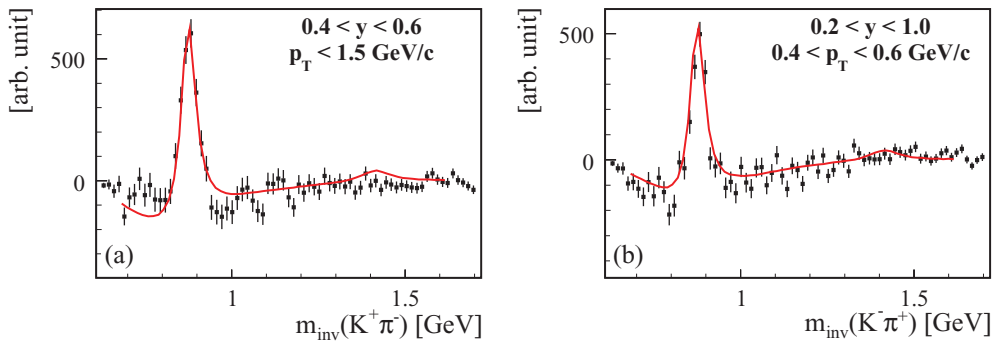

FIG. 6. (Color online) Examples of invariant-mass distributions for $K^+\pi^-$ (a) and $K^-\pi^+$ (b) after subtraction of mixed-event background in inelastic $p + p$ collisions. The curves show the fits with the sum of Breit-Wigner functions to describe the signals of the $K^*(892)^0$ and $K_2^*(1430)^0$ and the contributions from their reflections (see text).

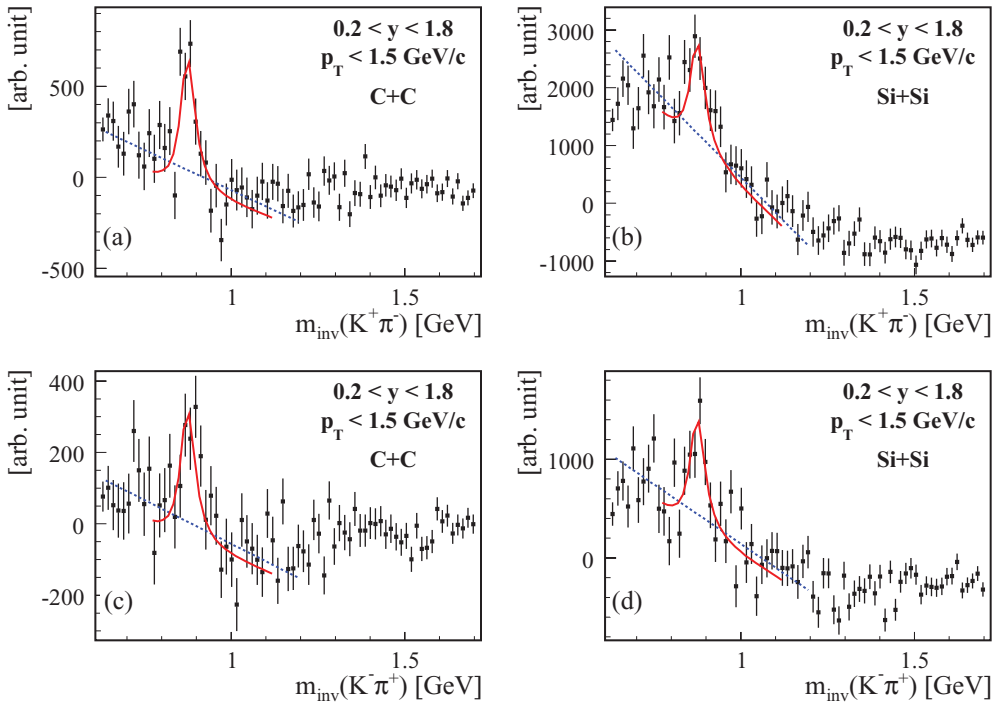

FIG. 7. (Color online) Invariant-mass distribution of $K^+\pi^-$ (a),(b) and $K^-\pi^+$ (c),(d) in the rapidity region $0.2 < y < 1.8$ and $p_T < 1.5$ GeV/c after subtraction of mixed-pair background. Results are plotted for C + C collisions in (a),(c) and for Si + Si collisions in (b),(d). The fitted residual background is shown by the dashed lines; the sum of fitted background and signal Breit-Wigner function is shown by the solid curves.

of $\sigma(p)/p^2 \approx (0.3\text{–}7) \times 10^{-4}$ (GeV/c)$^{-1}$ depending on track length.

Figure 1 shows a density plot of dE/dx as a function of momentum p for accepted positively (a) and negatively (b) charged particles showing bands for various particle species. K and π meson candidates were selected by requiring a momentum in the range $3 < p < 100$ GeV/c and a measured dE/dx value in a band of 2.5 and 3 standard deviations, respectively, around the expected mean values. Expected losses owing to the cuts are small (<2%) and no correction was applied. Systematic biases of the K^* yields from uncertainties in the fit of the Bethe-Bloch function are estimated to be below <5%.

Raw yields of the $K^*(892)^0$ and $\overline{K}^*(892)^0$ resonance states were extracted from the invariant-mass distributions calculated for $K^+\pi^-$ and $K^-\pi^+$ pair candidates, respectively. First, invariant-mass

$$m_{\text{inv}}(K\pi) = \sqrt{(E_K + E_\pi)^2 - (\vec{p}_K + \vec{p}_\pi)^2} \qquad (1)$$

distributions were computed for all selected $K^+\pi^-$ and $K^-\pi^+$ candidate pairs in the events. Next, similarly obtained distributions from pairs taken from different events of the same multiplicity class and normalized to the number of real pairs were subtracted to reduce the dominant contribution from combinatorial background. The resulting invariant-mass

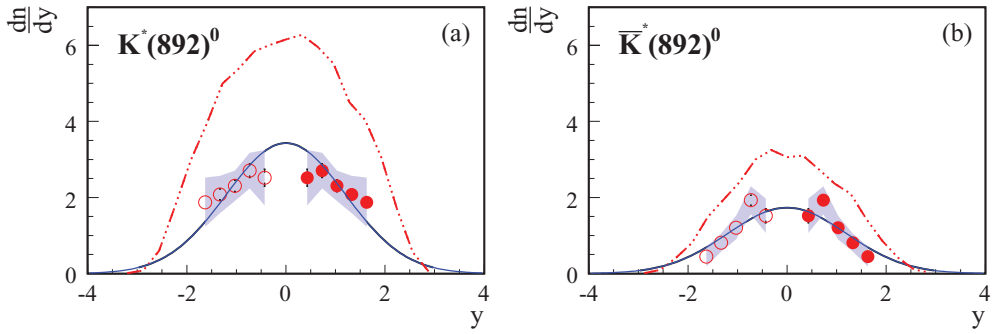

FIG. 8. (Color online) Rapidity distribution of $K^*(892)^0$ (a) and $\overline{K}^*(892)^0$ (b) integrated over p_T in central Pb + Pb collisions. Solid symbols represent the measurements; open symbols were obtained by reflection around midrapidity. The bars show statistical errors; the bands indicate systematic errors. Solid curves show fits of Gaussian functions for estimating total yields; dashed-dotted curves depict predictions of the UrQMD model [28].

TABLE I. Yields of $K^*(892)^0$ and $\overline{K}^*(892)^0$ per event in central Pb + Pb collisions as a function of rapidity y and integrated over transverse momentum. Both statistical (first) and systematic (second) errors are listed.

y	$\frac{dn}{dy}[K^*(892)^0]$	$\frac{dn}{dy}[\overline{K}^*(892)^0]$
0.3–0.6	$2.52 \pm 0.22 \pm 0.73$	$1.52 \pm 0.19 \pm 0.45$
0.6–0.9	$2.71 \pm 0.18 \pm 0.47$	$1.93 \pm 0.13 \pm 0.37$
0.9–1.2	$2.31 \pm 0.16 \pm 0.40$	$1.21 \pm 0.11 \pm 0.31$
1.2–1.5	$2.08 \pm 0.15 \pm 0.49$	$0.81 \pm 0.10 \pm 0.24$
1.5–1.8	$1.88 \pm 0.13 \pm 0.65$	$0.45 \pm 0.08 \pm 0.26$
Total yield (Gauss fit)	$10.3 \pm 0.4 \pm 2.5$	$5.2 \pm 0.3 \pm 1.7$

distributions are plotted in Fig. 2 for transverse momenta $p_T < 2.0$ GeV/c and the rapidity range $0.6 < y < 0.9$. The peaks owing to the $K^*(892)^0$ and $\overline{K}^*(892)^0$ resonance states are clearly seen above a strongly mass-dependent residual background. The mixing procedure preserves the inclusive single-particle phase space distributions, but destroys all correlations between particles. It therefore cannot fully describe the combinatorial background in real events, which is presumably partly shaped by effects such as energy and momentum conservation, as well as reflections from other resonance states. The raw numbers of $K^*(892)^0$ and $\overline{K}^*(892)^0$ were derived from fits to the mass distributions after the mixed-event background had been subtracted. The fit function was chosen as a sum of a linear or a second-order polynomial background and a Breit-Wigner distribution:

$$\frac{dN}{dm_{\text{inv}}} = C \cdot \frac{\Gamma}{\pi\left[(m_{\text{inv}} - m_0)^2 + \left(\frac{\Gamma}{2}\right)^2\right]}, \tag{2}$$

where m_0 and Γ are mass and width of the K^*, and C is a normalization factor. Examples of such fits in the rapidity range $0.6 < y < 0.9$ are shown in Fig. 2. The fits are seen to provide a good description of the mass distributions in the fit range $780 < m_{\text{inv}} < 1100$ MeV and result in $m_0 = 886 \pm 2$ MeV and $\Gamma = 49 \pm 6$ MeV for $K^*(892)^0$ and $m_0 = 891 \pm 2$ MeV and $\Gamma = 52 \pm 7$ MeV for $\overline{K}^*(892)^0$. The mass values are somewhat smaller than the world average of 895.94 ± 0.22 MeV [19] and were found not to depend significantly on rapidity or p_T as demonstrated by Figs. 3(a) and 3(b) [example for the $K^*(892)^0$ which provides the better statistical accuracy]. Scaling of the magnetic field value by the upper limit of its systematic uncertainty of ±1% changes the fitted mass value by about ±5 MeV. Thus, the observed mass shift is at the limit of significance. The STAR experiment at RHIC also found a similarly reduced mass [see Fig. 3(b)] but only for p_T below about 1 GeV/c [9]. The fitted width agrees well with the world average of 48.7 ± 0.8 MeV [19] (the invariant-mass resolution is about 6 MeV [20]). No significant variation with rapidity or p_T [see Figs. 3(c) and 3(d)] was found in agreement with results from STAR [9].

Correction factors for acceptance and reconstruction efficiency were derived from Monte Carlo simulations. $K^*(892)^0$ and $\overline{K}^*(892)^0$ were generated with realistic distributions in transverse momentum and rapidity and then passed through

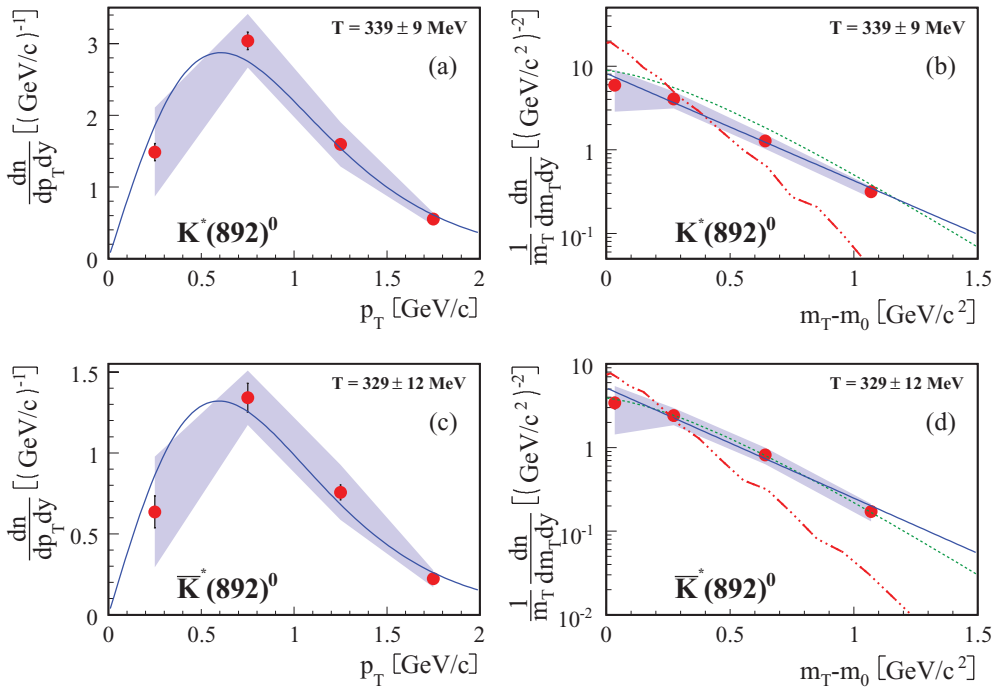

FIG. 9. (Color online) Differential yields in central Pb + Pb collisions as function of transverse momentum p_T (a),(c) and transverse mass m_T (b),(d) for $K^*(892)^0$ (a),(b) and $\overline{K}^*(892)^0$ (c),(d) in the rapidity interval $0.43 < y < 1.78$. The bars show statistical errors; the bands indicate systematic errors. Solid curves show results of exponential fits [Eq. (3), see text]. Dotted curves result from blast-wave calculations using the parameters fitted in Ref. [29]. The dashed-dotted curves depict predictions of the UrQMD model [28].

the NA49 simulation chain based on GEANT 3.21 [21] and a specific TPC signal simulation software. These signals were then added at the TPC signal level to the raw data of real events (embedding). Finally, the hybrid events were reconstructed and analyzed like real events. A matching step associated the reconstructed tracks with the originally generated tracks. Resulting invariant-mass spectra are plotted in Fig. 4 and demonstrate that neither the mass peak position nor its width are affected by the measuring resolution.

Correction factors for reconstruction inefficiencies, limited geometrical acceptance and in-flight decays were obtained by comparing the $K^*(892)^0$ and $\overline{K}^*(892)^0$ yields extracted from the reconstructed hybrid events to the generated yield. Resulting efficiencies for $K^*(892)^0 \to K^+\pi^-$ are shown as a function of rapidity and transverse momentum in Fig. 5 and range from 0.4 to 0.8. Values for $\overline{K}^*(892)^0 \to K^-\pi^+$ are the same within statistical errors. Efficiencies with embedding (solid symbols) are lower than those obtained by simulating only K^* (open symbols) but suggest only a modest effect of the high track density in the TPCs.

Differential $K^*(892)^0$ yields were obtained by fitting the invariant-mass spectra after subtraction of combinatorial background in bins of transverse momentum and rapidity. To ensure the stability of the fits the $K^*(892)^0$ mass and width were fixed to the world averages. The number of $K^*(892)^0$ in each bin was calculated as the integral of the Breit-Wigner function. Correction factors were then applied for the reconstruction efficiency and the decay branching ratio (66.7%).

Systematic errors were estimated by varying the identification criteria for kaons and the details of the fit procedure applied to the mass distributions. Increasing or decreasing the width of the dE/dx selection by half a standard deviation of the dE/dx measurements led to changes in the yields of around $\pm 7\%$. Extending or narrowing the mass range of the fit by 50 MeV or changing from a linear to a second-order polynomial background affected the results by about $\pm 10\%$. Other sources of uncertainty, such as using a mass value different from the world average or changing the inverse slope parameter T in the efficiency calculation, were much smaller. The total systematic error was estimated as half the range covered by the results obtained when varying the dE/dx cuts and the fitting procedure as just described. More details of the analysis procedure for Pb + Pb collisions can be found in Ref. [22].

B. $p + p$ collisions

For $p + p$ collisions the interaction vertex was determined from the backextrapolated tracks and the trajectory of the individual beam particle in the target, which was measured by the BPDs. To obtain a clean sample of $p + p$ collisions, only events with a successfully fitted vertex differing in position by less than ± 9 cm (± 5.5 cm for short target) in z-(beam-)direction from the target center and having a radial distance of less than 1 cm from the beam axis were accepted, thus minimizing contributions from interactions in the Mylar windows of the target vessel. From data taken with the liquid hydrogen removed from the target vessel ("empty-target runs") the remaining fraction of background events was estimated to be below 1% and therefore no correction was applied.

Correction procedures were devised to obtain the yield per inelastic $p + p$ collision. The efficiency and accuracy of vertex reconstruction using tracks backextrapolated from the TPCs vary with the charged-particle multiplicity of the event. The efficiency was derived from the probability that a successful vertex fit is obtained and that the fitted location fell inside the cuts. The corrections amount to 30% for events with three tracks, but rapidly drop to 6% for events with seven tracks. Furthermore, about 7% of the triggered events have no accepted tracks in the detector. Half of these can be attributed to the 1-mb contribution of elastic scattering events to the 28.3-mb trigger cross section; the other half are most likely attributable to singly diffractive events. To obtain the yield per triggered inelastic event, the number of events with tracks in the TPCs was scaled up by 3.5% for the per-event normalization.

A further correction was applied for the $14.4 \pm 1\%$ of inelastic events which do not give rise to a trigger [14]. Their contribution to the inclusive production cross section was found to generally depend on p_T, Feynman x, and the type of the produced particle under consideration [23]. However, for charged kaons only a weak rapidity and no significant p_T dependence was observed. For K^* resonance production we assume a similar behavior and thus estimate that, on average, the observed K^* yield should be scaled up by $5 \pm 1\%$. However, the number of events used for normalization has to

TABLE II. Yields $\frac{dn}{dp_T dy}$ of $K^*(892)^0$ and $\overline{K}^*(892)^0$ per event in central Pb + Pb collisions as a function of transverse momentum p_T in the rapidity interval $0.43 < y < 1.78$. Both statistical (first) and systematic (second) errors are shown for the differential yields. The inverse slope parameters T of exponential fits according to Eq. (3) are listed with their statistical errors.

p_T [GeV/c]	$\frac{dn}{dp_T dy}[K^*(892)^0]$ [(GeV/c)$^{-1}$]	$\frac{dn}{dp_T dy}[\overline{K}^*(892)^0]$ [(GeV/c)$^{-1}$]
0.0–0.5	$1.49 \pm 0.12 \pm 0.66$	$0.64 \pm 0.10 \pm 0.34$
0.5–1.0	$3.04 \pm 0.13 \pm 0.38$	$1.34 \pm 0.09 \pm 0.17$
1.0–1.5	$1.59 \pm 0.07 \pm 0.31$	$0.76 \pm 0.04 \pm 0.17$
1.5–2.0	$0.55 \pm 0.04 \pm 0.09$	$0.22 \pm 0.02 \pm 0.05$
T [GeV]	0.339 ± 0.009	0.329 ± 0.012

TABLE III. Yields $\frac{1}{m_T}\frac{dn}{dm_T dy}$ of $K^*(892)^0$ and $\overline{K}^*(892)^0$ per event in central Pb + Pb collisions as a function of transverse mass $m_T - m_0$ in the rapidity interval $0.43 < y < 1.78$. Both statistical (first) and systematic (second) errors are listed.

$m_T - m_0$ [GeV/c^2]	$\frac{1}{m_T}\frac{dn}{dm_T dy}[K^*(892)^0]$ [(GeV/c^2)$^{-2}$]	$\frac{1}{m_T}\frac{dn}{dm_T dy}[\overline{K}^*(892)^0]$ [(GeV/c^2)$^{-2}$]
0.034	$5.95 \pm 0.48 \pm 2.48$	$2.54 \pm 0.39 \pm 1.37$
0.272	$4.05 \pm 0.16 \pm 0.50$	$1.79 \pm 0.12 \pm 0.22$
0.642	$1.27 \pm 0.06 \pm 0.24$	$0.61 \pm 0.04 \pm 0.13$
1.070	$0.32 \pm 0.02 \pm 0.05$	$0.13 \pm 0.01 \pm 0.03$

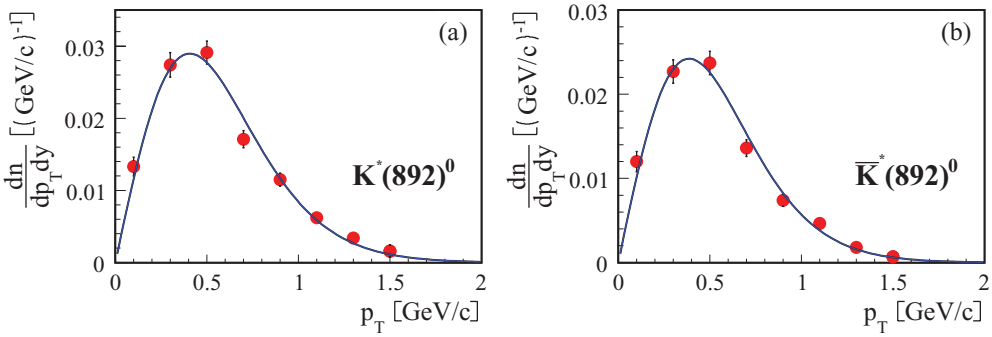

FIG. 10. (Color online) Transverse momentum distribution of $K^*(892)^0$ (a) and $\overline{K}^*(892)^0$ (b) for the rapidity interval $0.2 < y < 0.7$ in inelastic $p + p$ collisions at 158 GeV/c incident momentum. Only statistical errors are shown; the overall systematic error of normalization is 9%. Curves show results of fits with the exponential function Eq. (3).

be increased by 14.4% to obtain the yield per inelastic event. To account for the trigger loss we therefore scale down the measured $K^*(892)^0$ and $\overline{K}^*(892)^0$ yields per event as defined in the previous paragraph by $10 \pm 1\%$.

For $p + p$ reactions invariant-mass spectra could be extracted with much lower combinatorial background than for A + A collisions. Selected kaons and pions were required to have more than 30 points per track, a momentum in the interval $4 < p < 50$ GeV/c, a transverse momentum of $p_T \leqslant 1.5$ GeV/c, and a measured dE/dx value within $\pm 1.5\,\sigma_{dE/dx}$ around the expected dE/dx position. Pairs were entered into the invariant-mass distributions with the appropriate event-multiplicity-dependent correction factors. The background in the invariant-mass spectrum was determined by mixing kaons and pions from different events. This distribution was normalized to the same number of entries as the real event spectrum and subtracted, resulting in a small undershoot around the $K^*(892)^0$ signal (see Fig. 6). This undershoot structure is well described by simulations of invariant-mass distributions resulting from $K^*(892)^0$ decays and the contributions of the $K^*(892)^0$ decay products to the mixed event background [24] (see curves in Fig. 6). No additional subtraction of remaining background is necessary here. In the simulation an expected contribution from the $K_2^*(1430)^0$ (24% of the $K^*(892)^0$ yield [25]) was accounted for. Its inclusion does improve the description of the invariant-mass distribution, but does not influence the $K^*(892)^0$ yield. The fitted mass of the $K^*(892)^0$ was 892 ± 5 MeV, consistent with the world average [19]. The width was also found to agree with the world average.

Yields of the $K^*(892)^0$ and $\overline{K}^*(892)^0$ were extracted by fitting the normalization factor of the simulated invariant-mass distributions in bins of rapidity and transverse momentum. The simulation used the world average values for masses and widths and took into account the effect of geometrical acceptance and kaon decay in flight. Losses owing to reconstruction inefficiency are negligible in $p + p$ collisions. Global corrections were applied for dE/dx particle identification cuts and the decay branching fraction. Systematic errors were evaluated by changing track cuts of the selected kaons and pions and amount to 8% for the integrated yield. A conservative systematic error of 4% is assigned for the uncertainties of the vertex reconstruction efficiency and the trigger loss corrections. The final systematic error is taken as the quadratic sum of all these contributions and amounts to 9%. More details on the analysis procedure for $p + p$ collisions can be found in Ref. [26].

C. C + C and Si + Si collisions

The analysis of C + C and Si + Si collisions follows a strategy similar to that employed for Pb + Pb and $p + p$ collisions, however being limited by low statistics. The available number of events was not sufficient to extract rapidity and transverse mass distributions, but allowed only to estimate a total yield. $K^*(892)^0$ and $\overline{K}^*(892)^0$ invariant-mass spectra (see Fig. 7) were extracted in a wide range of rapidity $0.2 < y < 1.8$ and transverse momentum $p_T < 1.5$ GeV/c. Kaons and pions were selected in the momentum range of $4 < p < 50$ GeV/c and $p_T < 1$ GeV/c. The minimum number of points required per track was 50. Pions and kaons were identified by dE/dx within a band of typically ± 1.5 standard deviations around the Bethe-Bloch value. Both cuts were varied to estimate the systematic uncertainties.

TABLE IV. Yields $\frac{dn}{dp_T dy}$ of $K^*(892)^0$ and $\overline{K}^*(892)^0$ per event in inelastic $p + p$ collisions for the rapidity interval $0.2 < y < 0.7$ as a function of transverse momentum p_T with statistical errors. The systematic error of normalization (not shown) is 9%. The inverse slope parameters T of exponential fits according to Eq. (3) are also listed with statistical and systematic errors.

p_T (GeV/c)	$\frac{dn}{dp_T dy}$ [$K^*(892)^0$]	$\frac{dn}{dp_T dy}$ [$\overline{K}^*(892)^0$]
0.0–0.2	0.0133 ± 0.0013	0.0120 ± 0.0012
0.2–0.4	0.0274 ± 0.0017	0.0227 ± 0.0014
0.4–0.6	0.0291 ± 0.0016	0.0237 ± 0.0014
0.6–0.8	0.0171 ± 0.0012	0.0136 ± 0.0010
0.8–1.0	0.0115 ± 0.0009	0.00741 ± 0.00073
1.0–1.2	0.0062 ± 0.0007	0.00466 ± 0.00050
1.2–1.4	0.0034 ± 0.0005	0.00180 ± 0.00034
1.4–1.6	0.0016 ± 0.0008	0.00070 ± 0.00035
T (GeV)	$0.166 \pm 0.011 \pm 0.010$	$0.150 \pm 0.010 \pm 0.010$

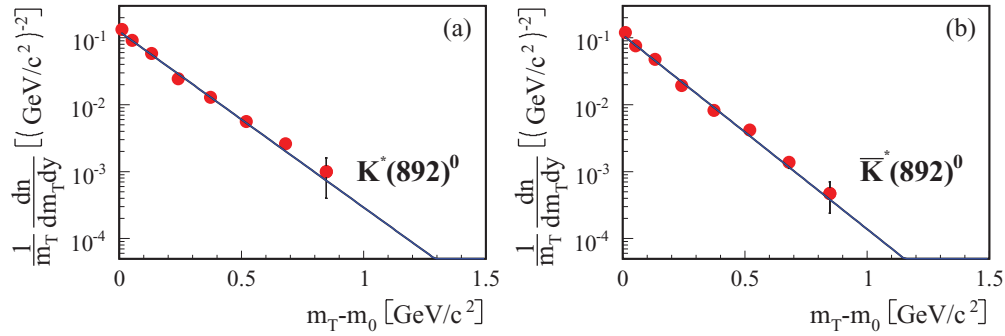

FIG. 11. (Color online) Transverse mass distribution of $K^*(892)^0$ (a) and $\overline{K}^*(892)^0$ (b) for the rapidity interval $0.2 < y < 0.7$ in inelastic $p + p$ collisions at 158 GeV/c incident momentum. Only statistical errors are shown; the overall systematic error of normalization is 9%. Curves show results of fits with the exponential function Eq. (3).

A similar strategy for invariant-mass spectra, background calculation, and signal extraction was used as for $p + p$ collisions. However, subtraction of the mass distributions from mixed events did not completely remove the combinatorial background, as can be seen from Fig. 7. The remaining background was parameterized as a straight line in the $K^*(892)$ mass region (dashed lines in Fig. 7). The signal was then obtained by fitting the sum of this linear background and the $K^*(892)$ line shape (using the world average values for mass and width [19]) including its reflections, as was done for $p + p$ reactions. The results of the fits are shown as the solid curves in Fig. 7.

The extracted raw yields were corrected for acceptance, the dE/dx identification cuts, and the decay branching fraction. The mean acceptance of $K^*(892)^0$ and $\overline{K}^*(892)^0$ in the selected wide phase space was calculated by Monte Carlo simulations assuming a width of the rapidity distribution similar to that of charged kaons and inverse p_T slopes similar to that of the ϕ meson [18] as its mass is close to that of the $K^*(892)$. A typical value of the mean acceptance requiring more than 100 points for both the pion and kaon track is 14%. Varying the assumptions on background shape and the kinematic distributions of the $K^*(892)$ changes the mean acceptance by 10% only. Extracted yields have statistical errors of 15%–20%. Varying background assumptions and selection criteria of kaons and pions, yields change by 15% at most. We thus assign a combined systematic and statistical error of 30%. More details on the analysis can be found in Ref. [26].

TABLE V. Yields $\frac{1}{m_T}\frac{dn}{dm_T dy}$ of $K^*(892)^0$ and $\overline{K}^*(892)^0$ per event in inelastic $p + p$ collisions for the rapidity interval $0.2 < y < 0.7$ as a function of $m_T - m_0$. Only statistical errors are shown. The systematic error of normalization (not shown) is 9%.

$\langle m_T \rangle - m_0$ (GeV/c^2)	$\frac{1}{m_T}\frac{dn}{dm_T dy}$ $[K^*(892)^0]$	$\frac{1}{m_T}\frac{dn}{dm_T dy}$ $[\overline{K}^*(892)^0]$
0.011	0.1331 ± 0.0132	0.1200 ± 0.0117
0.053	0.0914 ± 0.0054	0.0757 ± 0.0048
0.132	0.0583 ± 0.0032	0.0477 ± 0.0027
0.241	0.0244 ± 0.0018	0.0194 ± 0.0015
0.373	0.0129 ± 0.0010	0.0082 ± 0.0008
0.520	0.0056 ± 0.0006	0.0042 ± 0.0005
0.680	0.0026 ± 0.0004	0.00138 ± 0.00026
0.847	0.0010 ± 0.0006	0.00047 ± 0.00023

IV. RESULTS

A. Pb + Pb collisions

Yields of $K^*(892)^0$ and $\overline{K}^*(892)^0$ per event were extracted for the region of rapidity $0.3 < y < 1.8$ and transverse momentum $0 < p_T < 2.0$ GeV/c. Efficiency-corrected results are plotted as a function of rapidity y in Fig. 8 and listed in Table I. They include a small extrapolation in p_T beyond 2.0 GeV/c based on the exponential parametrization of the invariant p_T distribution using the temperature parameter T fitted in the measured p_T range (see below). The rapidity distributions decrease with increasing y and suggest a maximum at midrapidity in view of the forward-backward symmetry of the reaction.

The shapes of the rapidity distributions are not tightly constrained owing to the large errors and the restricted range covered by the measurements. We therefore derived estimates of total yields by fitting various shape funtions obtained from other reactions (Φ [27], K^+ and K^- [2]) and the UrQMD model. The resulting variation of the results is about 5%, well below the systematic errors from other sources discussed above. As the final result we give the average in Table I.

For obtaining distributions in transverse momentum yields were extracted in four p_T bins for the rapidity range $0.43 < y < 1.78$. The results for $\frac{dn}{dp_T dy}$ are plotted in panels (a),(c) of Fig. 9 and listed in Table II. From these measurements the yield as a function of transverse mass $m_T = \sqrt{p_T^2 + m_0^2}$ (where m_0 is the K^* mass) was calculated. The obtained values of $\frac{1}{m_T}\frac{dn}{dm_T dy}$ are shown in panels (b) and (d) of Fig. 9 and are listed in Table III. An exponential function,

$$\frac{1}{m_T}\frac{dn}{dm_T dy} = A \cdot e^{-\frac{m_T}{T}}, \tag{3}$$

was fitted to these measurements, where T is the inverse slope parameter and A a normalization constant. The resulting values of $T = 339 \pm 9$ MeV for $K^*(892)^0$ and $T = 329 \pm 12$ MeV for $\overline{K}^*(892)^0$ are much larger than for kaons, but closer to that

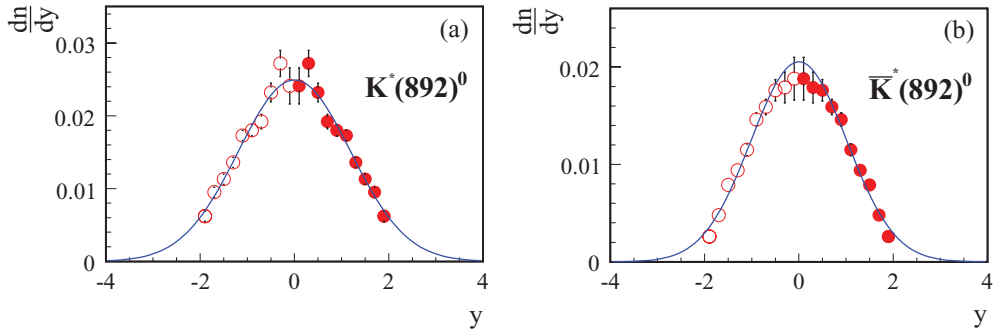

FIG. 12. (Color online) Rapidity distributions for $K^*(892)^0$ (a) and $\overline{K}^*(892)^0$ (b) integrated over $p_T < 1.5$ GeV/c in inelastic $p + p$ collisions at 158 GeV/c incident momentum. Only statistical errors are shown; the overall systematic error of normalization is 9%. Curves show fits with a Gaussian function centered at midrapidity $y = 0$ (χ^2 per degree of freedom 1.1 and 1.4, respectively).

for the higher-mass ϕ meson [27]. Moreover, $\frac{1}{m_T}\frac{dn}{dm_T dy}$ seems to exhibit a convex shape in the logarithmic representation of Fig. 9. This behavior may be attributable to the participation of the K^* in the strong radial flow [29]. Indeed, a blast-wave calculation, also shown in Figs. 9(b) and 9(d) by dotted curves, provides a good description of the K^* spectra using parameters fitted to pion, kaon, proton, and antiproton spectra ($T = 93$ MeV, $\rho_0 = 0.91$ [29]). Alternatively, the convex shape could be attributable to the attenuation of the K^* in the fireball, which is expected to be strongest for low values of p_T.

B. $p + p$ collisions

For $p + p$ reactions results are presented as yields per inelastic reaction. Transverse momentum spectra (see Fig. 10 and Table IV) were extracted in a rapidity range of $0.2 < y < 0.7$. The range was chosen as close to midrapidity as the acceptance for the $K^*(892)$ allows. The m_T spectra (see Fig. 11 and Table V) show a thermal shape which can be well described by an exponential function [Eq. (3)] with an inverse slope parameter $T = 166 \pm 15$ MeV for $K^*(892)^0$ and 150 ± 14 MeV for $\overline{K}^*(892)^0$, respectively. These values are consistent with those found for other mesons in $p + p$ collisions [26], indicating the absence of radial flow in these reactions. The p_T-integrated rapidity spectrum (see Fig. 12 and Table VI) was extracted for $p_T < 1.5$ GeV/c, except for the last rapidity bin $1.8 < y < 2.0$, which had a reduced range of $p_T < 1.2$ GeV/c because of the upper momentum limit imposed by the dE/dx identification procedure. The range $0 < p_T < 1.5$ GeV/c contains 99.1% of all $K^*(892)$ (for $T = 160$ MeV). The total yields (listed in Table VII) were extracted by fitting a Gaussian distribution centered at $y = 0$ to the rapidity distribution. The resulting widths of the rapidity distributions and the midrapidity yields are listed in Table VI. The extracted width of the rapidity distribution is consistent with the one for charged kaons [23]. The extracted yields (extrapolated fraction 9% and 4%, respectively) fit well into the trend of results from $p + p$ collisions at higher and lower energies (see Ref. [26] for a more detailed comparison).

TABLE VI. Yields of $K^*(892)^0$ and $\overline{K}^*(892)^0$ per event with statistical errors in inelastic $p + p$ collisions as a function of rapidity y and integrated over $p_T < 1.5$ GeV/c. The systematic error of normalization (not shown) is 9%. Also listed are the widths σ_y, the central rapidity yields $\frac{dn}{dy}|_{y=0}$ and the total yields obtained from Gaussian fits with statistical and systematic errors.

y	$\frac{dn}{dy}[K^*(892)^0]$	$\frac{dn}{dy}[\overline{K}^*(892)^0]$
0.0–0.2	0.0241 ± 0.0025	0.0188 ± 0.0022
0.2–0.4	0.0272 ± 0.0018	0.0179 ± 0.0016
0.4–0.6	0.0232 ± 0.0013	0.0176 ± 0.0011
0.6–0.8	0.0192 ± 0.0010	0.0159 ± 0.0008
0.8–1.0	0.0180 ± 0.0008	0.0146 ± 0.0007
1.0–1.2	0.0173 ± 0.0007	0.0115 ± 0.0006
1.2–1.4	0.0136 ± 0.0007	0.0094 ± 0.0005
1.4–1.6	0.0113 ± 0.0007	0.0079 ± 0.0005
1.6–1.8	0.0095 ± 0.0007	0.0048 ± 0.0004
1.8–2.0	0.0062 ± 0.0007	0.0026 ± 0.0004
σ_y	$1.17 \pm 0.03 \pm 0.07$	$1.01 \pm 0.02 \pm 0.06$
$\frac{dn}{dy}\|_{y=0}$	$0.0257 \pm 0.0031 \pm 0.0023$	$0.0183 \pm 0.0027 \pm 0.0016$
Total yield	$0.0741 \pm 0.0015 \pm 0.0067$	$0.0523 \pm 0.0010 \pm 0.0047$

C. C + C and Si + Si collisions

Owing to the limited number of recorded events only total yields per event could be estimated (see Sec. III C). The results with their statistical and sytematic uncertainties are listed in Table VII.

V. DISCUSSION OF RESULTS

Both $K^*(892)^0$ [$\overline{K}^*(892)^0$] and K^+ [K^-] contain an antistrange (strange) valence quark in addition to a light (anti-) quark and should therefore be similarly sensitive to the strangeness content of the produced matter. The ratio of total yields $\langle K^*(892)^0\rangle/\langle\overline{K}^*(892)^0\rangle$ is about 2 in C + C, Si + Si, and Pb + Pb collisions (see Table VII) and is similar to the ratio $\langle K^+\rangle/\langle K^-\rangle \approx 2.0$ [2,18], as expected. The yields per wounded nucleon are compared graphically in Fig. 13(a).

TABLE VII. Total yields of $K^*(892)^0$ and $\overline{K}^*(892)^0$ in inelastic $p+p$ and in central C + C, Si + Si, and Pb + Pb collisions at 158A GeV beam energy. Statistical and systematic errors were added in quadrature. In addition, model predictions are listed from HGM (fit A of Ref. [12]) and UrQMD 1.3 [28] (predictions are for the $K^+\pi^-$ and $K^-\pi^+$ decay channels, respectively, and were scaled by 3/2 to account for the branching ratio).

Reaction		$p+p$	C + C	Si + Si	Pb + Pb
Centrality		Minimum bias	15.3%	12.2%	23.5%
$\langle N_W \rangle$		2	14 ± 2	37 ± 3	262 ± 6
$\langle K^*(892)^0 \rangle$	This analysis	0.0741 ± 0.0069	0.8 ± 0.24	2.2 ± 0.66	10.3 ± 2.5
	HGM	0.074	0.964	2.76	25.1
	UrQMD	0.076	0.74	2.25	22.2
$\langle \overline{K}^*(892)^0 \rangle$	This analysis	0.0523 ± 0.0048	0.43 ± 0.14	1.3 ± 0.4	5.2 ± 1.7
	HGM	0.041	0.455	1.33	12.5
	UrQMD	0.043	0.41	1.19	9.5

This quantity seems to increase from $p+p$ to C + C and Si + Si collisions and then to decrease to central Pb + Pb collisions. This behavior may result from an interplay between strangeness enhancement in nucleus-nucleus collisions and the interaction of the $K^*(892)$ and its decay products in the produced fireball.

Because kaons and $K^*(892)$ both contain the same valence quarks, the system size dependence of the ratios $\langle K^* \rangle / \langle K^+ \rangle$ and $\langle \overline{K}^* \rangle / \langle K^- \rangle$ is expected to be sensitive mostly to the interactions in the surrounding medium while the effect of strangeness enhancement should approximately cancel. As can be seen from Fig. 13(b), the ratios decrease by about a factor of 2 from C + C and Si + Si reactions to central Pb + Pb collisions and by about a factor of 3 when taking $p+p$ reactions as the reference. Thus, $K^*(892)^0$ yields seem to be strongly affected by interactions in the produced fireball with destruction dominating regeneration. Published measurements from the STAR collaboration at RHIC energies [9] show a weaker suppression of the $\langle K^* \rangle / \langle K^+ \rangle$ ratio for central Cu + Cu and Au + Au collisions compared to inelastic $p+p$ reactions of only about 30%.

Microscopic models of hadron production in nucleus-nucleus collisions have been used to study the modification of resonance yields during the space-time evolution of the fireball. In the UrQMD model [11], particle production proceeds via string excitation and decay at high energies and evolves further by interactions and coalescence in the produced matter. During the model simulations the full history for each particle is recorded, thus making it possible to study the phenomena of destruction and regeneration of resonance states [28,30], which was first considered in Ref. [7]. For comparison with our measurements, we extracted the predicted yields in the $K^+\pi^-$ and $K^-\pi^+$ decay channels, respectively, and scaled them by 3/2 to take into account the decay branching ratio as was done for the data. The measured rapidity spectra of $K^*(892)^0$ and $\overline{K}^*(892)^0$ in central Pb + Pb collisions at 158A GeV are compared to results from UrQMD model calculations in Fig. 8 (dashed-dotted curves). While one observes good agreement for the shape of the rapidity distributions, yields are overpredicted by roughly a factor of two. Moreover, the predicted transverse mass distributions are steeper than those of the data [see dashed-dotted curves in Figs. 9(b) and 9(d)].

Inspection of the particle histories in the simulated UrQMD events indicates that of the originally produced $K^*(892)^0$ [$\overline{K}^*(892)^0$] about 2% (2%) in $p+p$, 12% (13%) in central C + C, 23% (27%) in central Si + Si and 44% (62%) in central Pb + Pb collisions are lost owing to in-medium interactions and decay (rescattering of the decay products).

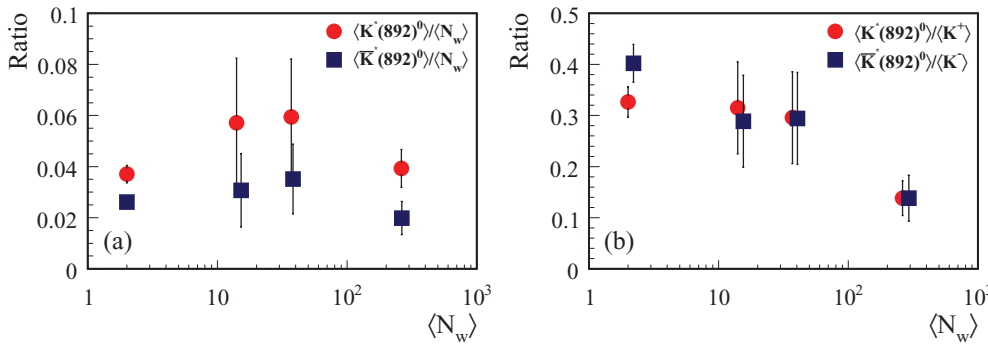

FIG. 13. (Color online) (a) Yields per wounded nucleon $K^*(892)^0/\langle N_W \rangle$ (dots) and $\overline{K}^*(892)^0/\langle N_W \rangle$ (squares) versus size of the collision system. (b) Ratios $\langle K^*(892)^0 \rangle / \langle K^+ \rangle$ (dots) and $\langle \overline{K}^*(892)^0 \rangle / \langle K^- \rangle$ (squares) versus size of the collision system ($p+p$, C + C, Si + Si, and Pb + Pb collisions). Total kaon yields were taken from Refs. [2,18,23] and appropriately scaled by $\langle N_W \rangle$. For evaluating error bars the quadratic sums of statistical and systematic errors were used.

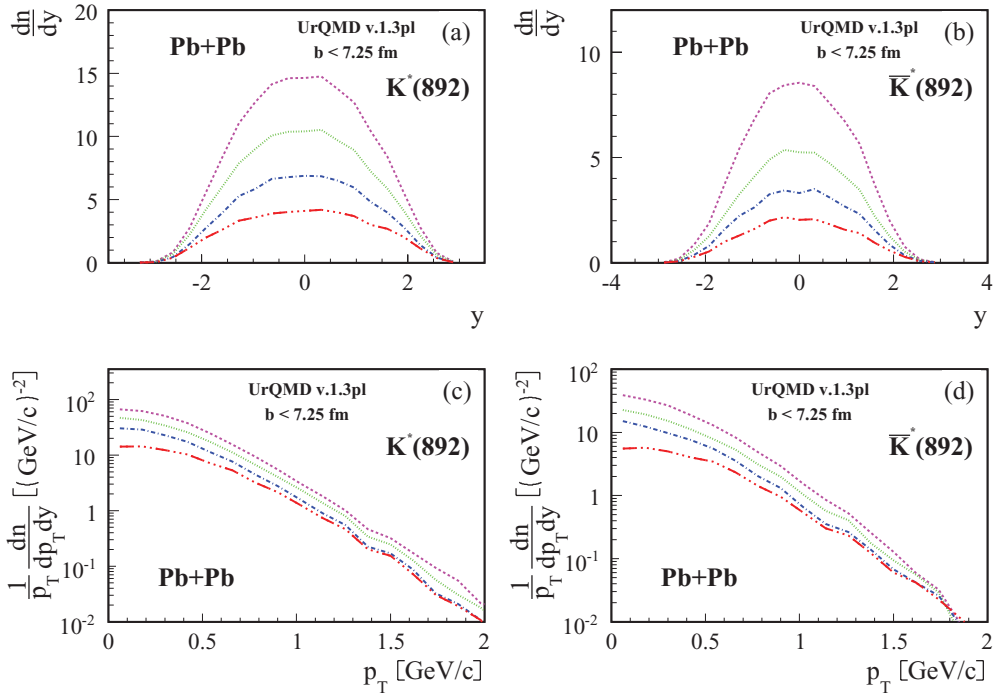

FIG. 14. (Color online) Predictions of the UrQMD model version 1.3p1 [28] for the 23.5% most central Pb + Pb collisions at 158A GeV: distributions of rapidity (a),(b) and transverse momentum p_T (c,d) in the rapidity interval $0.43 < y < 1.78$ of $K^*(892)^0$ (a),(c) and $\overline{K}^*(892)^0$ (b),(d). The curves show the successive reduction of yields owing to various interaction mechanisms of the $K^*(892)^0$ and $\overline{K}^*(892)^0$ and their decay daughters in the fireball (see text). Note that the final results show the yield predictions for the $K^+\pi^-$ and $K^-\pi^+$ decay channels, respectively. The curves in Figs. 8 and 9 were obtained by scaling these by 3/2.

The contributions of the various mechanisms are illustrated by the curves shown in Fig. 14. The first reduction is attributable to reinteractions of the K^* in the fireball medium and the second reduction is the effect of the decay branching ratio into $K^+\pi^-$ and $K^-\pi^+$, respectively. The last reduction is caused by the scattering of the K^* decay daughters in the medium. The model calculations thus suggest a sizable duration of the hadronic phase of the fireball to allow for such reinteractions.

Predictions of the UrQMD model for total yields are listed in Table VII. The agreement with the measurements for $p + p$, C + C, and Si + Si reactions suggests that UrQMD reproduces the absorption effects in these smaller systems. In contrast, predicted total $K^*(892)^0$ and $\overline{K}^*(892)^0$ yields for central Pb + Pb collisions exceed the experimental results by roughly a factor of two. This might imply that the lifetime of the hadronic phase is larger than suggested by the model calculation.

The statistical HGM was found to provide a good fit to total yields of stable hadrons produced in elementary $e^+ + e^-$, $p + p$, and nucleus + nucleus collisions using as adjustable parameters the hadronization temperature $T_{\rm chem}$, the baryochemical potential μ_B, and a strangeness saturation parameter γ_s [12,31]. The predictions for $K^*(892)$ yields

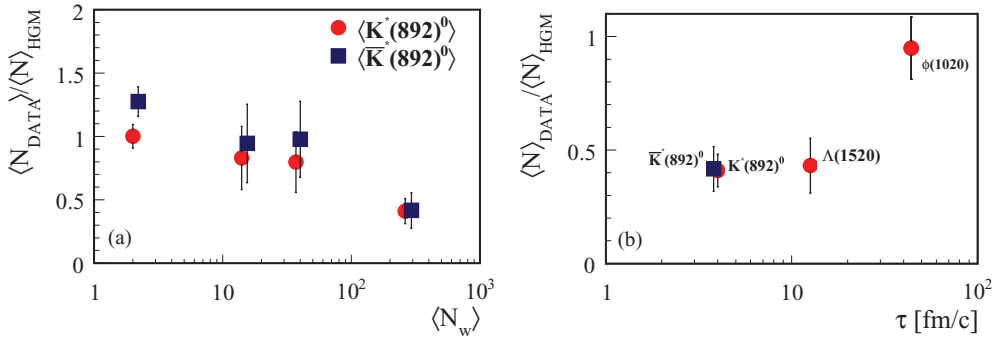

FIG. 15. (Color online) (a) Ratio of measured total yields of $K^*(892)^0$ (dots) and $\overline{K}^*(892)^0$ (squares) to statistical HGM predictions [12] versus the size of the collision system ($p + p$, C + C, Si + Si, and Pb + Pb collisions). (b) Ratio of measured yield in central Pb + Pb collisions to the statistical HGM prediction for $K^*(892)^0$ (dot), $\overline{K}^*(892)^0$ (square), ϕ meson [27], and preliminary measurement of $\Lambda(1520)$ [32] versus the lifetime τ of the resonance state. For evaluating error bars the quadratic sums of statistical and systematic errors were used.

(which were not included in the fit of the model parameters) in $p+p$ and nucleus + nucleus collisions are compared to the measurements in Fig. 15(a). One finds that the HGM predictions are consistent with the measurements for $p+p$ and light-nuclei collisions, but exceed by more than a factor of 2 the observed yields in central Pb + Pb reactions.

Yields of several resonance states were investigated by the NA49 collaboration, namely of $K^*(892)^0$, $\Lambda(1520)$ [32], and the ϕ meson [27]. The ratios between the measured yields and the predictions of the HGM model are plotted in Fig. 15(b) versus the respective lifetimes (3.91, 12.7, and 46.5 fm/c). The suppression with respect to the HGM predictions seems to get stronger with decreasing lifetime of the resonance. This suggests that a large part of the reduction of the $K^*(892)^0$ yield may be caused by rescattering of its decay daughters during the hadronic stage of the fireball and implies that this stage lasts for a time (estimated about 6 fm/c in Ref. [29]) at least comparable to the lifetime of the resonance.

Alternatively, one may reconsider the assumption of simultaneous chemical freeze-out of the hadrons from the fireball at a unique temperature. In the statistical HGM the yield ratio of two hadrons with identical strangeness, isospin, and baryon number makes it possible to estimate the freeze-out temperature T_{fo} (in the Boltzmann approximation, and neglecting feed-down from resonances) as

$$T_{fo} = (m_2 - m_1)/\ln\left[\left(\frac{2J_1+1}{2J_2+1}\right)\left(\frac{m_1}{m_2}\right)^{\frac{3}{2}}\left(\frac{N_2}{N_1}\right)\right], \quad (4)$$

where m_1, m_2 are the masses, J_1, J_2 the spins, and N_1, N_2 the produced multiplicities. Inserting the numbers for the pairs $\Lambda(1520)$, Λ and $K^*(892)^0$, $K^\pm$ one obtains apparent freeze-out temperatures of 90 MeV for $\Lambda(1520)$ and 100 MeV for $K^*(892)^0$, respectively. The chemical freeze-out temperature fitted to the yields of stable hadrons is $T_{\rm chem} = 155$ MeV [12]. This would lead to the conclusion that short-lived resonances freeze-out at the end of the fireball evolution when the temperature has fallen below that for stable hadrons.

VI. SUMMARY

Production of the $K^*(892)^0$ and $\overline{K}^*(892)^0$ resonances was studied via their $K^+\pi^-$ and $K^-\pi^+$ decay modes in central Pb + Pb, Si + Si, C + C, and inelastic $p+p$ collisions at 158A GeV ($\sqrt{s_{NN}} = 17.3$ GeV) with the NA49 detector at the CERN SPS. Transverse momentum and rapidity distributions were obtained and total yields were estimated. The following conclusions were reached.

(i) The yield of $K^*(892)^0$ exceeds that of $\overline{K}^*(892)^0$ by about a factor of two. This observation can be understood from the similar ratio of the K^+ and K^- yields and the valence quark composition of these mesons.

(ii) The yield of $K^*(892)^0$ and $\overline{K}^*(892)^0$ per wounded nucleon appears to increase from $p+p$ to C + C and Si + Si collisions and then tends to decrease to central Pb + Pb reactions. This behavior seems to reflect an interplay between strangeness enhancement in nucleus-nucleus collisions and attenuation of $K^*(892)^0$ and $\overline{K}^*(892)^0$ in the produced fireball.

(iii) The ratios $\langle K^*(892)^0\rangle/\langle K^+\rangle$ and $\langle \overline{K}^*(892)^0\rangle/\langle K^-\rangle$ decrease strongly with increasing size of the colliding nuclei. These ratios are expected to be mostly sensitive to interactions of the $K^*(892)^0$ and its decay daughters with the produced dense matter. The decrease of the ratios suggests a substantial duration of the hadronic stage of the fireball.

(iv) The UrQMD model, although including rescattering of $K^*(892)^0$ and $\overline{K}^*(892)^0$ and their decay daughters in the hadronic phase, is not able to provide a quantitative description of $K^*(892)^0$ production in nucleus-nucleus collisions at SPS energies.

(v) Yields of $K^*(892)^0$ mesons in central Pb + Pb collisions are about a factor of 2.5 below the predictions of the statistical HGM using parameters fitted to the yields of stable hadrons.

In summary, the predicted suppression of $K^*(892)^0$ yields [7] was observed in central Pb + Pb collisions at the SPS. It was found to be stronger at SPS than at RHIC energies. More comprehensive studies of the energy and system-size dependence of the suppression of hadron resonance production will help to better understand the hadronization process and the evolution of the high-density matter droplet created in nucleus-nucleus collisions.

ACKNOWLEDGMENTS

This work was supported by US Department of Energy Grant No. DE-FG03-97ER41020/A000, the Bundesministerium für Bildung und Forschung, Germany (Grant No. 06F137), the German Research Foundation (Grant No. GA 1480/2-1), the Polish Ministry of Science and Higher Education (Grants No. 1 P03B 006 30, No. 1 P03B 127 30, No. 0297/B/H03/2007 /33, No. N N202 078735, and No. N N202 204638), the Hungarian Scientific Research Foundation (Grants No. T068506, No. A08-77719, and No. A08-77815), the Janos Bolyai research grant, the Bulgarian National Science Fund (Grant No. Ph-09/05), the Croatian Ministry of Science, Education and Sport (Project No. 098-0982887-2878), and Stichting FOM, the Netherlands.

[1] U. Heinz and M. Jacob, arXiv:nucl-th/0002042.
[2] C. Alt *et al.*, Phys. Rev. C **77**, 024903 (2008).
[3] M. Gaździcki, M. Gorenstein, and P. Seyboth, Acta Phys. Pol. B **42**, 2705 (2011).
[4] J. Rafelski and B. Müller, Phys. Rev. Lett. **48**, 1066 (1982).
[5] M. Gaździcki and M. Gorenstein, Acta Phys. Pol. B **30**, 2705 (1999).
[6] R. Rapp and J. Wambach, Adv. Nucl. Phys. **25**, 1 (2000).

[7] G. Torrieri and J. Rafelski, Phys. Lett. B **509**, 239 (2001); Z. Xu (STAR Collaboration), Nucl. Phys. B **698**, 607c (2002).
[8] C. Adler *et al.*, Phys. Rev. C **66**, 061901R (2002).
[9] J. Adams *et al.*, Phys. Rev. C **71**, 064902 (2005); M. Aggarwal *et al.*, *ibid.* **84**, 034909 (2011); S. Dash (STAR Collaboration), J. Phys. G **35**, 104057 (2008).
[10] P. Seyboth, J. Phys. G **35**, 104008 (2008); R. Barton *et al.*, *ibid.* **27**, 367 (2001).
[11] S. Bass *et al.*, Prog. Part. Nucl. Phys. **41**, 255 (1998); M. Bleicher *et al.*, J. Phys. G **25**, 1859 (1999).
[12] F. Becattini, J. Manninen, and M. Gaździcki, Phys. Rev. C **73**, 044905 (2006) (Results of fit A were used for comparisons.)
[13] S. Afanasiev *et al.*, Nucl. Instrum. Methods Phys. Res., Sect. A **430**, 210 (1999).
[14] C. Alt *et al.*, Eur. Phys. J. C **45**, 343 (2006).
[15] A. Białas, M. Błeszyński, and W. Czyż, Nucl. Phys. B **111**, 461 (1976). (Note that N_W is often referred to less precisely as the number of participants. N_W does not include nucleons participating only in secondary interactions.)
[16] K. Werner, Phys. Rep. **232**, 87 (1993).
[17] A. Laszlo, CERN EDMS Id 885329.
[18] C. Alt *et al.*, Phys. Rev. Lett. **94**, 052301 (2005).
[19] K. Nakamura *et al.* (Particle Data Group), J. Phys. G **37**, 075021 (2010).
[20] C. Alt *et al.*, Phys. Rev. C **73**, 034910 (2006).
[21] Geant *Detector Description and Simulation Tool*, CERN Program Library Long Writeup W5013.
[22] M. Słodkowski, Ph.D. thesis, Warsaw University of Technology, 2008, CERN EDMS Id 999736.
[23] T. Anticic *et al.*, Eur. Phys. J. C **68**, 1 (2010).
[24] D. Drijard, H. Fischer, and T. Nakada, Nucl. Instrum. Methods **225**, 367 (1984).
[25] T. Aziz *et al.*, Z. Phys. C **30**, 381 (1986).
[26] C. Höhne, Ph.D. thesis, Marburg University, 2003, CERN EDMS Id 816035. (Note that the corrections for inelastic events not accepted by the trigger or having no tracks in the TPCs were revised.)
[27] C. Alt *et al.*, Phys. Rev. C **78**, 044907 (2008).
[28] S. Vogel and M. Bleicher, arXiv:nucl-th/0505027; S. Vogel, (private communication) (2008). (Version 1.3p1 was used to calculate the predictions.)
[29] C. Alt *et al.*, Phys. Rev. C **77**, 064908 (2008).
[30] M. Bleicher and J. Aichelin, Phys. Lett. B **530**, 81 (2002).
[31] F. Becattini and U. Heinz, Z. Phys. C **76**, 269 (1997).
[32] V. Friese (NA49 collaboration), Nucl. Phys. A **698**, 487 (2002); C. Markert, Ph.D. thesis, Frankfurt University, 2001, CERN EDMS Id 816027.